

promoting access to White Rose research papers



Universities of Leeds, Sheffield and York
<http://eprints.whiterose.ac.uk/>

This is a copy of the final published version of a paper published via gold open access in **Cement and Concrete Research**.

This open access article is distributed under the terms of the Creative Commons Attribution Licence (<http://creativecommons.org/licenses/by/4.0/>) which permits unrestricted use, distribution, and reproduction in any medium, provided the original work is properly cited.

White Rose Research Online URL for this paper:
<http://eprints.whiterose.ac.uk/86458>

Published paper

Gardner, L.J., Bernal, S.A., Walling, S.A., Corkhill, C.L., Provis, J.L. and Hyatt, N.C. (2015) *Characterisation of magnesium potassium phosphate cements blended with fly ash and ground granulated blast furnace slag*. *Cement and Concrete Research*, 74. 78 - 87. Doi: 10.1016/j.cemconres.2015.01.015



Characterisation of magnesium potassium phosphate cements blended with fly ash and ground granulated blast furnace slag



Laura J. Gardner, Susan A. Bernal, Samuel A. Walling, Claire L. Corkhill, John L. Provis, Neil C. Hyatt*

Immobilisation Science Laboratory, Department of Materials Science and Engineering, University of Sheffield, Sir Robert Hadfield Building, Portobello Street, Sheffield S1 3JD, UK

ARTICLE INFO

Article history:

Received 28 August 2014

Accepted 19 January 2015

Available online 16 May 2015

Keywords:

Microstructure (B)

SEM (B)

Fly ash (D)

Granulated blast furnace slag (D)

Chemically Bonded Ceramics (D)

ABSTRACT

Magnesium potassium phosphate cements (MKPCs), blended with 50 wt.% fly ash (FA) or ground granulated blast furnace slag (GBFS) to reduce heat evolution, water demand and cost, were assessed using compressive strength, X-ray diffraction (XRD), scanning electron microscopy (SEM) and nuclear magnetic resonance (NMR) spectroscopy on ^{25}Mg , ^{27}Al , ^{29}Si , ^{31}P and ^{39}K nuclei. We present the first definitive evidence that dissolution of the glassy aluminosilicate phases of both FA and GBFS occurred under the pH conditions of MKPC. In addition to the main binder phase, struvite-K, an amorphous orthophosphate phase was detected in FA/MKPC and GBFS/MKPC systems. It was postulated that an aluminium phosphate phase was formed, however, no significant Al–O–P interactions were identified. High-field NMR analysis of the GBFS/MKPC system indicated the potential formation of a potassium-aluminosilicate phase. This study demonstrates the need for further research on these binders, as both FA and GBFS are generally regarded as inert fillers within MKPC.

© 2015 The Authors. Published by Elsevier Ltd. This is an open access article under the CC BY license (<http://creativecommons.org/licenses/by/4.0/>).

1. Introduction

Magnesium potassium phosphate cement (MKPC) is a clinker-free acid–base cement, in which the mechanical strength development is a direct result of the rapid formation of cementitious hydrogel type products [1]. The chemical reaction resulting in the formation of MKPCs (Eq. (1)) is based on the dissolution of MgO and KH_2PO_4 reacting in solution to form struvite-K ($\text{MgKPO}_4 \cdot 6\text{H}_2\text{O}$), which is isostructural to struvite ($\text{NH}_4\text{MgPO}_4 \cdot 6\text{H}_2\text{O}$) [2] and is naturally cementitious. In 2003, struvite-K was classified as a distinct mineral species by the Commission of New Mineral and Mineral Names, International Mineralogical Association (CNMNM-IMA) after it was discovered naturally in two locations; Binntal, Switzerland and the Styria region of Austria [3].



When compared to conventional Portland cements, MKPCs have advantageous properties including near-neutral pH, low water demand, low drying shrinkage and high early compressive strength [4]. These properties make MKPCs remarkably versatile, and this cementing system has been used for rapid repair of damaged roads, bridges and runways [5], in conditioning various nuclear waste streams containing reactive metals [6,7] and in dental castings with antibacterial properties [8].

In practical application, MKPC binders are frequently blended (up to 50 wt.% replacement) with fly ash (FA) from the coal combustion

process to reduce their production cost, reduce water demand of the paste, and lower the exothermic output of the acid–base reaction which avoids cracking of the hardened paste. The inclusion of FA in MKPC enhances the workability of the binder via the “ball-bearing effect” of the spherical particles [6,9–11]. Several studies [6,12,13] based on FA/MKPC blended binders have suggested that FA simply acts as a diluent or inert filler, that modifies the aesthetics of MKPC to be compatible to traditional Portland cement, which has been deemed important for rapid-repair applications [9]. Conversely, others hypothesise that FA replacement promotes high mechanical strength in FA/MKPC binders, as a consequence of the formation of a secondary amorphous phase containing silicon-phosphate bonds [12,14]. This is commensurate with the work of Wilson and Nicholson [1], who suggested that aluminosilicate glass can react with phosphoric acid to form a strong phosphate bonded cement. It is conceivable that the glassy aluminosilicate fraction of the FA reacts in the initially acidic environment of the MKPC, forming a secondary phase intermixed with struvite-K. If this occurs, it could result in a matrix of higher density that would be more impermeable to water, have a higher mechanical strength [15,16] and provide additional sites for sorption of radionuclides, which would be of importance for application in the encapsulation of radioactive wastes. However, previous studies have not identified additional crystalline or amorphous reaction products, for example by powder X-ray diffraction or Fourier transform infrared spectroscopy, although the compressive strength and setting characteristics were altered in MKPC with the inclusion of FA [17].

Ground granulated blast furnace slag (GBFS) produced in the iron-making process is a FA alternative that could be used as a diluent within MKPC binders. GBFS/MKPC blended binders are novel and little open

* Corresponding author. Tel.: +44 114 222 5470; fax: +44 114 222 594.
E-mail address: n.c.hyatt@sheffield.ac.uk (N.C. Hyatt).

literature is available concerning their properties. However, it should be noted that crystalline and amorphous blast furnace slags have been previously employed as filter/sorbent materials to remove phosphates from wastewater systems such as constructed wetlands and soil infiltration systems [18–20]. As such, it is conceivable that slag–phosphate interactions could occur within this system and potentially lead to the formation of secondary reaction products.

The reaction of supplementary cementitious materials (SCMs), FA and GBFS, at the pH and chemical speciation conditions reached within MKPC binders, is largely unclear; detailed chemical or microstructural characterisation of secondary cementitious phases forming in FA/MKPC or GBFS/MKPC binders has not yet been reported, and there is a lack of evidence regarding whether or not the dissolution of FA or GBFS particles occurs (and to what extent) within MKPC-based binders. It is therefore imperative to develop an in-depth mechanistic understanding of the role of FA and GBFS within the phase assemblage of MKPC binders.

In this study, FA/MKPC and GBFS/MKPC binders were investigated via mechanical testing (compressive strength), XRD, SEM, ^{25}Mg magic angle spinning (MAS) NMR, ^{27}Al MAS NMR, ^{29}Si MAS NMR, ^{31}P MAS NMR, $^{31}\text{P}\{^1\text{H}\}$ cross polarisation (CP/MAS) NMR and ^{39}K MAS NMR spectroscopy techniques, with the aim of providing the first detailed characterisation of these systems.

2. Experimental programme

2.1. Materials

MgO was sourced from Richard Baker Harrison Ltd in the form of Dead Burnt Magnesia (DBM) at 90% purity. KH_2PO_4 was provided by Prayon UK as Food Grade E340 MKP, and the certificate of analysis purity was >99%. FA was supplied by CEMEX as PFA BS EN 450-1S [21]. Ground granulated blast furnace slag (GBFS) from Scunthorpe Steelworks was supplied by Hanson Cements according to the established specifications of Sellafield Limited for use in the UK nuclear industry, and is a blend of finely-ground and coarser-ground materials. Granular boric acid (H_3BO_3) was sourced from Fisher Scientific UK (CAS number 10043-35-3, laboratory grade) with a purity of >99.5%, and used as a retarder. The chemical compositions of MgO, FA and GBFS determined by X-ray fluorescence (XRF) oxide analysis are given in Table 1. The powder properties (particle size distribution, fineness, specific surface area and density) are reported in Table 2.

2.2. Mix design

The formulations used throughout this study involve the addition of boric acid as a setting retarder to ensure that a workable paste is formed, as without a retarder similar magnesium phosphate systems have been reported to set within 20 min [22], which is not desirable for large-scale industrial applications. The addition of dead-burnt MgO (low reactivity) and supplementary cementitious materials (FA or GBFS; which act as diluents) has also been reported to further extend the setting time of the acid–base reaction [6,23]. The formulations to produce blended

Table 1
Composition of raw materials determined by XRF oxide analysis (precision ± 0.1 wt.%).

Compound (wt.%)	MgO	FA	GBFS
Na_2O	<0.1	1.1	0.4
MgO	88.9	1.7	7.9
Al_2O_3	1.7	25.2	12.0
SiO_2	4.3	50.2	36.6
P_2O_5	<0.1	0.3	<0.1
K_2O	0.1	3.6	0.7
CaO	2.1	2.4	40.2
Fe_2O_3	1.5	9.3	0.4
Total	98.8	93.8	98.3

Table 2

Characterisation of raw materials using PSD, Blaine fineness, BET surface area and density measurements.

Material	d_{10} (μm)	d_{50} (μm)	d_{90} (μm)	Blaine fineness (m^2/kg)	BET (m^2/kg)	Density (kg/m^3)
MgO	3.2 ± 0.1	24.4 ± 0.3	63.8 ± 0.6	329 ± 16	563 ± 72	3471 ± 1
FA	2.7 ± 0.1	14.0 ± 0.3	66.1 ± 3.5	560 ± 10	2258 ± 10	2329 ± 5
GBFS	1.6 ± 0.1	16.0 ± 0.1	1465 ± 15	497 ± 17	993 ± 72	2885 ± 5

MKPC pastes are shown in Table 3; a 1.7 MgO:1 KH_2PO_4 molar ratio (based on previous research [6]) with a water-to-solids (w/s) ratio of 0.24 was used, with additions of 50 wt.% of either FA or GBFS, and 2 wt.% H_3BO_3 .

The precursors (MgO, KH_2PO_4 , SCMs and H_3BO_3) were mixed initially for 10 min in a Kenwood benchtop mixer at low speed. Afterwards, the slurry was transferred to a high shear Silverson mixer and mixed for an additional 10 min at 4000 rpm to achieve a homogenous paste. The binders were poured into centrifuge tubes or steel moulds and cured for 28 days in an environmental chamber at 20 °C and 95% relative humidity until testing.

2.3. Analytical methods

Compressive strength was determined from triplicate 50 mm cube specimens after 3, 7 and 28 days of curing using a Controls Automax 5.0 machine at a loading rate of 0.25 MPa/s. Paste samples cured for 28 days were crushed and subsequently ground using an agate mortar and passed through a 63 μm sieve prior to powder XRD analysis using a STOE STADI P diffractometer with an image plate detector and Cu $\text{K}\alpha$ radiation (1.5406 Å); diffraction patterns were collected between $10^\circ < 2\theta \leq 50^\circ$. SCM-blended MKPC samples were polished and carbon coated for analysis using a Jeol JSM 6400 SEM at a 20 kV accelerating voltage and a working distance of 15 mm. Elemental maps were collected using a Link ISIS EDS (energy dispersive X-ray spectrometer) detector.

Solid-state NMR spectra were collected on a Varian VNMRS 400 (9.4 T) spectrometer using either a probe for 4 mm o.d. zirconia rotors (^{27}Al , ^{31}P) or 6 mm o.d. zirconia rotors (^{29}Si). ^{27}Al MAS NMR spectra were collected at 104.198 MHz and a spinning speed of 14 kHz, employing a pulse width of 1 μs (25°), a relaxation delay of 0.2 s, and with a minimum of 7000 scans. ^{29}Si MAS NMR spectra were collected at 79.435 MHz at a spinning speed of 6.8 kHz and employed a pulse duration of 4.7 μs (90°) and a relaxation delay of 1.0–5.0 s, with a minimum of 1200 scans. ^{31}P MAS NMR spectra were collected at 161.874 MHz at a spinning speed of 10.0 kHz with a pulse duration of 4.4 μs (90°) and relaxation times of 10 and 300 s, with a minimum of 110 and 4 scans, respectively. $^{31}\text{P}\{^1\text{H}\}$ CP/MAS NMR spectra were collected at 161.874 MHz at a spinning speed of 10 kHz with a pulse duration of 4.4 μs , acquisition time of 30.0 ms at a recycle time of 1.0 s, and a minimum of 120 scans. ^{27}Al , ^{29}Si and ^{31}P chemical shifts are referenced to external samples of 1.0 M aqueous $\text{Al}(\text{NO}_3)_3$, tetramethylsilane (TMS), and 85% H_3PO_4 , respectively.

Solid-state NMR spectra for ^{25}Mg and ^{39}K nuclei were collected on a Bruker Advance III 850 (19.96 T) spectrometer using 4 mm o.d. zirconia rotors. ^{25}Mg MAS NMR spectra were collected at 52.05 MHz at a spinning speed of 10.0 kHz with a pulse duration of 5.0 μs (90°) and recycle time of 2.0 s for 5800 scans. ^{25}Mg MAS NMR chemical shifts were

Table 3

Formulation of MKPC pastes based on a 0.24 water/solids ratio, using a 500 g batch size to ± 0.1 g precision [24].

Blend	MgO (g)	KH_2PO_4 (g)	H_2O (g)	FA (g)	GBFS (g)	H_3BO_3 (g)
MKPC	132.3	262.8	96.0	–	–	9.8
FA/MKPC	77.8	154.6	96.0	165.0	–	6.6
GBFS/MKPC	77.8	154.6	96.0	–	165.0	6.6

referenced to an external sample of MgO; the chemical shift of MgO (26 ppm) is defined with respect to the hydrated Mg^{2+} ion at $\delta = 0$ ppm as a primary reference [25]. ^{39}K MAS NMR spectra were collected using an echo sequence at 39.7 MHz, spectra were collected at a spinning speed of 15.0 kHz, a pulse duration of 15.0 μs (90°) and a recycle time of 2.0 s for 29,900 scans. ^{39}K MAS NMR chemical shifts were referenced to solid KBr, which has a chemical shift of 0 ppm with respect to the hydrated K^+ ion [26]. ^{25}Mg and ^{39}K simulations were performed using Bruker TopSpin 3.2 software [27] considering the second-order quadrupolar interaction for the central transition only.

3. Results and discussion

3.1. Compressive strength

The compressive strength of blended MKPC binders varied depending on the supplementary cementitious material added, as shown in Fig. 1. The compressive strength values of the FA/MKPC binder were comparable with data available for similar systems [6,28]. The GBFS/MKPC was observed to have superior mechanical properties compared to the FA/MKPC binder at all curing ages investigated. At day 28, there was a significant (10 MPa) difference between the FA/MKPC (24 MPa) and GBFS/MKPC (34 MPa) binders. The powder properties (Table 2) indicate that FA has a much narrower particle size distribution and is, in general, finer than the GBFS; the angular GBFS particles may be expected to interlock much better with the matrix than the spherical FA particles. However, this physical interlocking of the GBFS, due to particle packing effects [29], is unlikely to be the sole cause of the significant differences observed in mechanical performance identified in these binders. The FA/MKPC binder achieved comparable compressive strength values to the pure MKPC binder (Fig. 1) whereas the GBFS/MKPC binder was notably stronger. During testing, it was observed that the failure mode of MKPC was via viscoelastic deformation, rather than brittle fracture as in the FA/MKPC and GBFS/MKPC binders. This suggested that a possible chemical interaction between GBFS, FA and MKPC influenced the cementitious properties of the binder.

3.2. Powder X-ray diffraction

The diffraction patterns of the anhydrous GBFS and FA, along with the hardened GBFS/MKPC and FA/MKPC binders cured for 28 days, are shown in Fig. 2. In the anhydrous GBFS, traces of åkermanite ($\text{Ca}_2\text{MgSi}_2\text{O}_7$, PDF #76-841) were observed, whilst in unreacted FA, quartz (SiO_2 , PDF #11-252) and mullite ($\text{Al}_4\text{Si}_2\text{O}_{13}$, PDF #15-776) were identified. Diffuse scattering was identified, in FA between $15^\circ < 2\theta \leq 25^\circ$ and in GBFS between $25^\circ < 2\theta \leq 35^\circ$, which is associated

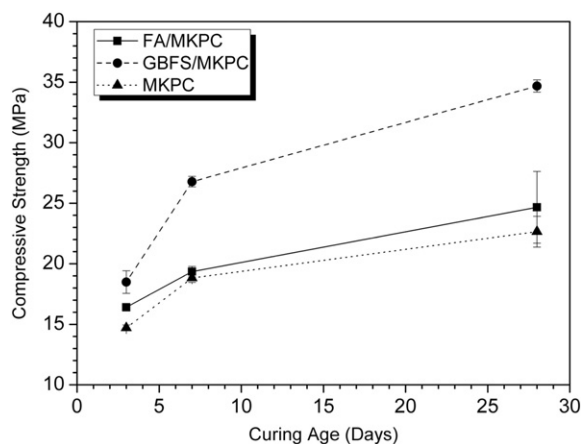


Fig. 1. Compressive strength of MKPC, GBFS/MKPC and FA/MKPC, as a function of curing time, the error bars are equivalent to ± 1 standard deviation.

with the X-ray amorphous aluminosilicate (FA) and calcium aluminosilicate (GBFS) glassy fractions that constitute the bulk material. Struvite-K ($\text{MgKPO}_4 \cdot 6\text{H}_2\text{O}$, PDF #75-1076) was found to be the main crystalline product forming in MKPC binders.

Traces of periclase (MgO , PDF #45-946) were also identified in the MKPC binders, as MgO was added in excess (1.7:1 Mg/P ratio) of the stoichiometric proportions to ensure the conversion of all phosphate to struvite-K. In the pure MKPC system, the use of a stoichiometric ratio of MgO to KH_2PO_4 has been found to give complete reaction with no residual MgO visible in XRD [30,31]. Crystalline secondary products were not observable in the MKPC blended either with FA or GBFS, and the degree of crystallinity of the struvite-K was found to be high.

3.3. Scanning electron microscopy

Backscattered electron images of FA/MKPC and GBFS/MKPC binders are shown in Fig. 3, where the formation of a continuous struvite-K phase embedded with large struvite-K crystallites can be seen in both systems. The embedded particles of struvite-K, with a laminar habit, appeared to be highly cracked in polished sections, due to dehydration under vacuum for analysis. Angular light grey particles correspond to unreacted GBFS (Fig. 3A), whilst spherical particles of varying sizes (Fig. 3B) are FA particles. A similar microstructure has previously been reported for FA/MKPC [6]; however, there are no reports of the microstructure of GBFS/MKPC binders in the open literature. The large struvite-K crystals are known mainly to occur in systems prepared using boric acid to retard the setting reaction [22], which therefore allows time for crystal growth within the adhesive binder [1].

3.3.1. Elemental mapping – GBFS/MKPC

In the GBFS/MKPC binder, a homogeneous distribution of Mg and P throughout the sample was observed in EDX maps (Fig. 4), consistent with the formation of crystalline struvite-K as the main binding phase of the system. Embedded unreacted MgO (Fig. 4) particles were identified, consistent with XRD data in Fig. 2. Angular particles of various sizes rich in Ca, Al and Si (Fig. 4) correspond to the unreacted calcium aluminosilicate glassy fraction present in GBFS particles. The Al and Si EDX maps (Fig. 4) show incorporation of these elements in the binding matrix, indicating that dissolution of GBFS had occurred. It was hypothesised that any free Al in the binder could preferentially form a second phosphate phase, within the struvite-K matrix. GBFS dissolution and subsequent reaction to form a secondary phase would explain the

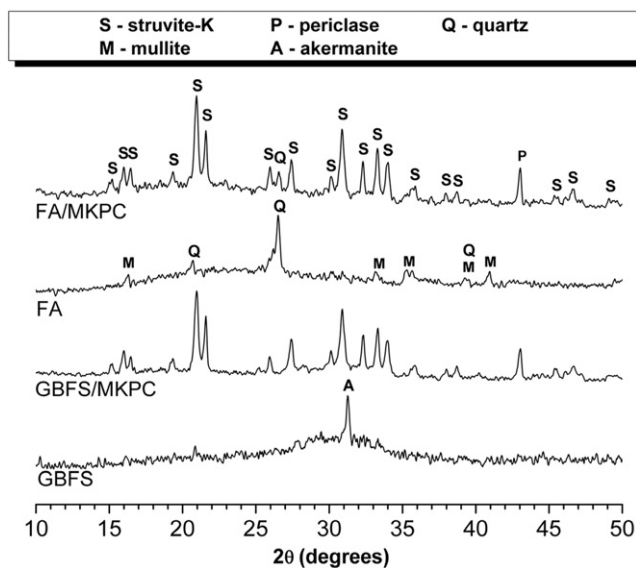


Fig. 2. X-ray diffraction patterns of GBFS/MKPC and FA/MKPC pastes after 28 days of curing.

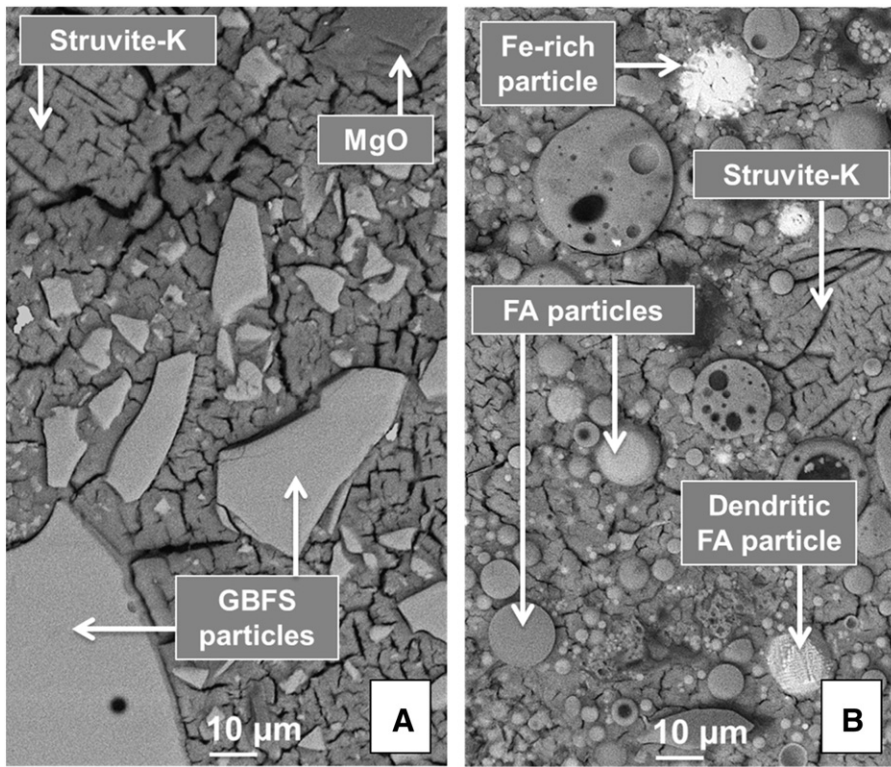


Fig. 3. Backscattered electron micrographs of (A) GBFS/MKPC and (B) FA/MKPC hardened pastes after 28 days of curing.

enhanced strength development of the binder [11] as a result of filling pores in the matrix. The “area of interest” in Fig. 4 shows an embedded GBFS particle immediately neighbouring a region rich in Al, Si and P, which may be a secondary reaction product.

Slags have previously been utilised as sorbents for phosphate removal from wastewater systems, and the mechanism for this process is controlled by the pH: at $\text{pH} \leq 6$, the mechanism is phosphate adsorption onto the surface of the slag particles [19] whereas at $\text{pH} \geq 8$, the

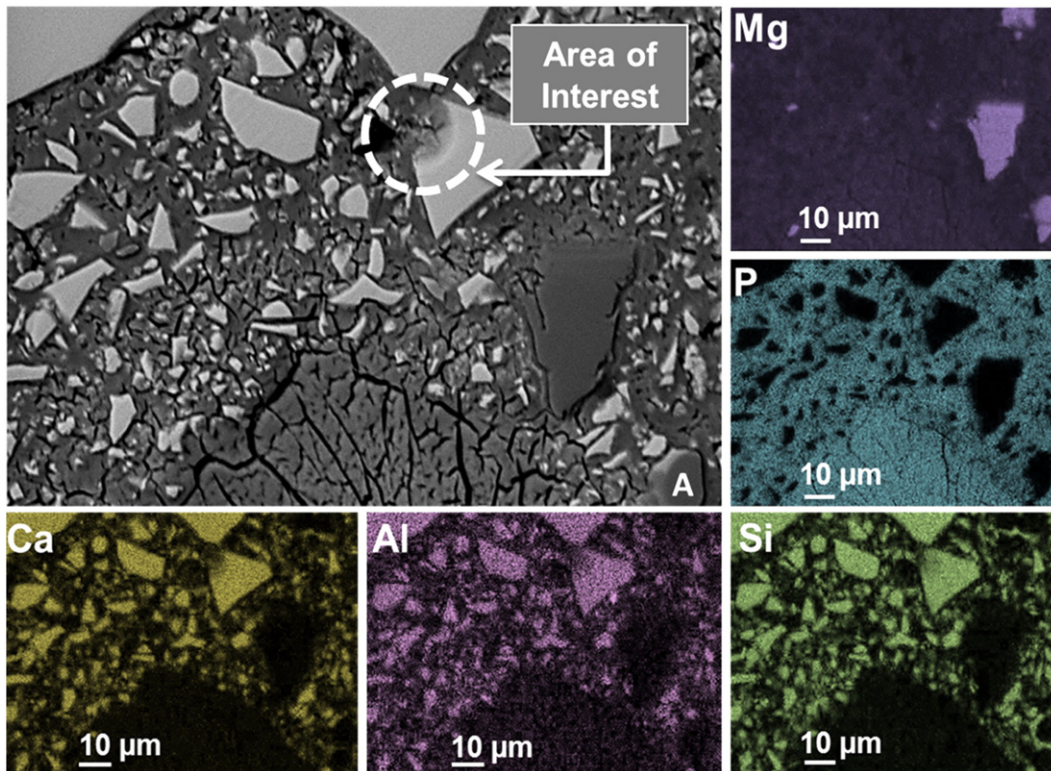


Fig. 4. Backscattered electron image and elemental maps of hardened GBFS/MKPC paste after 28 days of curing.

phosphate precipitates as calcium phosphates [20]. In the GBFS/MKPC binder, the majority of the Ca (Fig. 4) appeared to be retained within the unreacted GBFS particles with no evidence for the formation of calcium phosphates, consistent with the near-neutral pH conditions of the blended MKPC binder. The feature labelled as “A” in Fig. 4 shows a region associated with a remnant MgO grain that contains a minor but significant amount of Ca (2.1 wt.%, Table 1) and Si (4.3 wt.%, Table 1) as determined by bulk XRF of the MgO. This suggests that the MgO particles are ingrained with calcium silicate impurities, which were identified via grey-scale differences of the MgO grain. The Ca and Si impurities appeared to remain intact and hence, it was inferred that dissolution of Ca and Si from MgO does not occur in this system.

3.3.2. Elemental mapping – FA/MKPC

In the production of FA there is a negligible exchange of mass between particles, due to the nature of the coal combustion process. Therefore, FA particles have a wide variance in local composition, mineralogy and particle size, and this leads to a variable rate of reaction between particles [32]. Evidence of reaction of the FA particles within MKPC is shown in Fig. 3B, which illustrates the variation in FA reactivity, as several medium-sized (10–30 μm) particles have undergone partial reaction identified as surface dimpling [33,34], where smaller particles with a similar depth of attack on their surfaces may have undergone full reaction/dissolution. The separation of Fe-rich and Al–Si-rich phases within fly ash particles can occur as a result in different glass dissolution rates under alkaline conditions, resulting in etching of the Al–Si rich matrix to form insoluble Fe-rich dendritic particles [35]. However, we believe the particle in Fig. 5, was created during the cooling of the raw FA due to the perfect alignment of the dendritic phase with the circumference of the particle. The complete dissolution of the particle wall was observed in the FA particle (feature labelled “A” in Fig. 5) as a direct result of the near-neutral conditions of the FA/MKPC binder. It is postulated that preferential dissolution of Al–Si phases occurred, which could result in the formation of secondary reactions, whilst the identification of the Fe-rich phases present in FA particles (e.g. hematite) [36] suggests that they do not take part in any secondary reactions. Recent work evaluating FA/MKPC binders [14] speculated the formation of an amorphous phase coating the FA particles, which was proposed to be a silicon-phosphate phase. This postulation was drawn from BSE micrographs and small differences in XRD reflections compared to a pure MKPC binder. However, the elemental composition of this phase could not be confirmed and no supplementary analysis techniques were employed to investigate its presence.

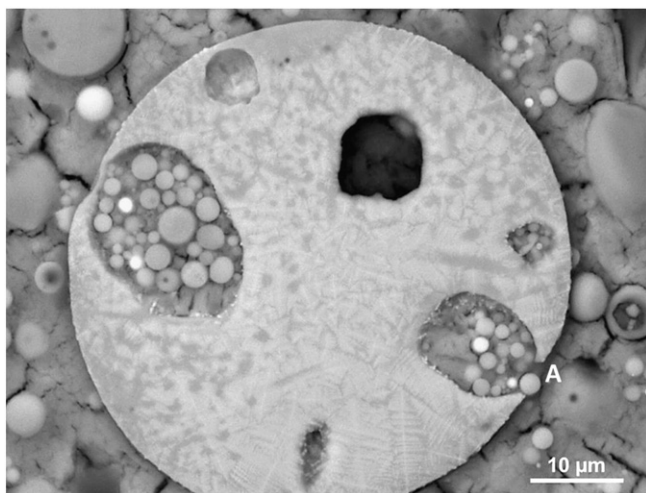


Fig. 5. Backscattered electron micrograph of a single FA particle showing prominent Al and Si dissolution resulting in phase separation leaving dendritic Fe-rich phases.

A highly dense microstructure was identified in FA/MKPC binders (Fig. 6); large struvite-K crystals (Fig. 6) were found to be surrounded by FA cenospheres. Similarly to GBFS/MKPC, unreacted MgO grains were evident throughout the matrix, and appeared to act as nucleation sites for struvite-K formation. A transition zone between the large struvite-K crystallite and the matrix was also observed, where small FA cenospheres agglomerated in the boundary of the struvite-K. This is indicative of a chemical interaction between the components. The Ca present in the FA/MKPC matrix (Fig. 6) appeared to be associated with Ca impurities within unreacted MgO grains (2.1 wt.% by XRF analysis of MgO, Table 1) rather than from the siliceous fly ash which has a Ca content of 2.4 wt.% (XRF analysis of FA, Table 1). The unreacted MgO grains were also found to be associated with silicon impurities (4.3 wt.% by XRF analysis of MgO, Table 1), potentially a calcium silicate impurity. The composition of MgO particles could potentially lead to dissolution of Ca and Si into the matrix to form secondary reaction products; however it is postulated that dissolution of the MgO impurity would not be the dominant contribution of free Si. The main binding matrix was observed to be significantly enriched in Al and Si (Fig. 6), dissolution of the aluminosilicate FA particles may have occurred within this system leading to the formation of a secondary product.

3.4. Nuclear magnetic resonance spectroscopy

^{27}Al MAS NMR spectra are known to clearly show three distinct Al coordination environments (Al^{IV} , Al^{V} and Al^{VI}), which for cements are located at chemical shifts between 52 to 80 ppm, 30 to 40 ppm and –10 to 15 ppm, respectively [25]. Two Al environments were identified in the ^{27}Al MAS NMR spectrum of unreacted GBFS, as shown in Fig. 7A. The first, and dominant site represents a broad Al^{IV} environment centred at 56 ppm, assigned to the aluminosilicate glassy fraction of the slag [37]. The second Al environment can be assigned to a minor band in the Al^{VI} region centred at 11 ppm, which may be attributed to a minor octahedral Al environment in the slag glass. In comparison, the GBFS/MKPC binder (Fig. 7A) has a narrower and slightly more deshielded Al^{IV} region than the unreacted slag, with a resonance centred at 54 ppm. The minor Al^{VI} environment in the GBFS/MKPC binder appeared to be more prominent than the unreacted GBFS. This may simply be because of a reduction in the intensity of the underlying resonance in this region during reaction.

The change in the Al^{IV} region in the GBFS/MKPC binder can be assigned to the remaining unreacted slag, which can undergo selective dissolution at the pH conditions reached in these binders (and thus display an apparent shift in its peak position as one or more of the multiple Al environments present are selectively removed). The potential formation of a highly cross-linked secondary phase, more likely an aluminosilicate type product, can also be indicated by such a shift, where the Al selectively leached from the slag remains in tetrahedral coordination but shows a more ordered nature than in the unreacted slag glass. In blended Portland cement and alkali-activated slag systems, the Al^{IV} region usually sharpens upon reaction due to the formation of an Al-substituted calcium silicate hydrate (C-(A)-S-H) [38] type gel. In non-cross-linked C-A-S-H type phases, the chemical shift of tetrahedrally coordinated Al occurred at 74 ppm [39–42], when ^{27}Al spectra were collected at the magnetic field used in the present study. The fact that the reaction product peak here is located far from 74 ppm indicated that formation of a C-A-S-H product did not occur in the GBFS/MKPC binder.

In the Al^{VI} region (–10 to 15 ppm), the most evident difference between the GBFS/MKPC and GBFS ^{27}Al MAS NMR spectra was the presence of a high intensity band centred at –9.5 ppm in the reacted material that was not present in the unreacted GBFS. This resonance can be assigned to the secondary reaction product forming in the GBFS/MKPC binder, which must be present at a very significant concentration to display such a clear NMR signal. The resonance is more shielded (more negative chemical shift) than the resonances which have been assigned to Al^{VI} in the literature for condensed and intermediate alumina,

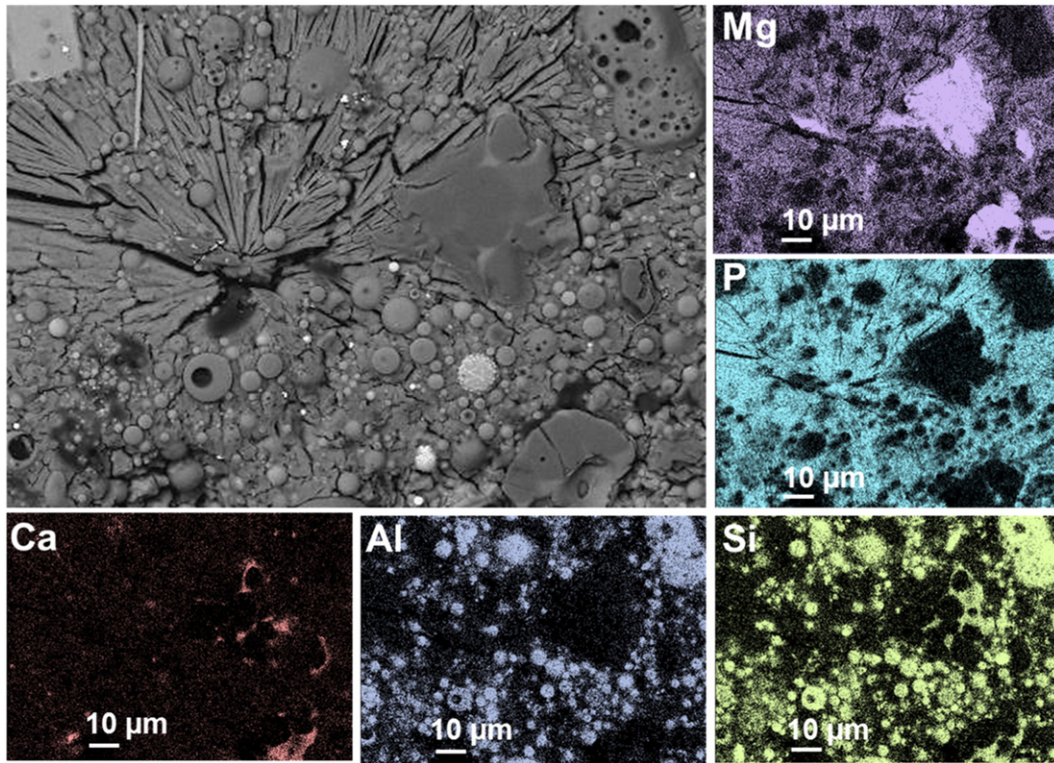


Fig. 6. Backscattered electron micrograph and elemental maps of hardened FA/MKPC paste after 28 days of curing.

aluminium hydroxide polymorphs and aluminosilicates [37,43,44], and Al-rich hydrous reaction products forming in GBFS-blended Portland cement [45], which are all usually identified between 0 and 13 ppm. An aluminium phosphate phase may potentially be formed as a result of chemical interactions between the GBFS and MKPC components. Aluminium-phosphate bonds are typically observed in ^{27}Al NMR spectra between 45 ppm and -25 ppm, with three main phosphate environments: $\text{Al}(\text{OP})_4$ centred at ~ 40 ppm, $\text{Al}(\text{OP})_5$ centred at ~ 10 ppm, and $\text{Al}(\text{OP})_6$ centred at ~ -20 ppm [25]. Accordingly, the additional

signal at -9.5 ppm in the GBFS/MKPC binder could possibly be attributed to an $\text{Al}(\text{OP})_6$ -containing phase, however, the ^{31}P NMR spectra in Fig. 8 call such an interpretation into question, as will be discussed in the following section.

Fig. 7B shows the ^{27}Al MAS NMR of unreacted FA and the FA/MKPC binder. The unreacted FA was found to have two main Al environments, Al^{IV} and Al^{VI} , centred at 47 ppm and -5 ppm, respectively. The band at -5 ppm can be assigned to mullite [46,47], as identified by XRD (Fig. 1), whilst the broad band centred at 47 ppm can be assigned to the

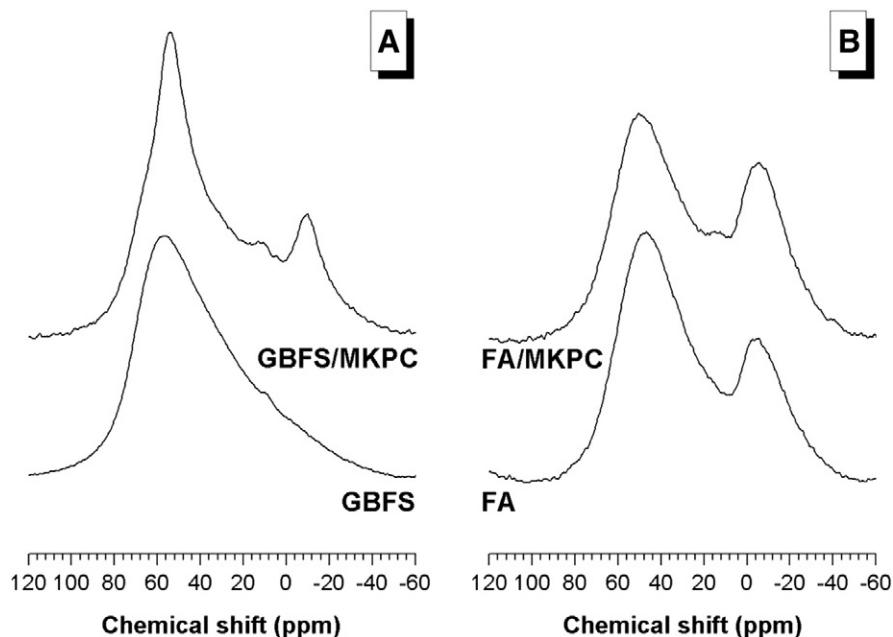


Fig. 7. ^{27}Al MAS NMR spectra (9.4 T, 14 kHz) for (A) unreacted GBFS and GBFS/MKPC hardened paste, and (B) unreacted FA and FA/MKPC hardened paste.

tetrahedral resonance of mullite (reported to be at 46 ppm [47]) and the highly cross-linked aluminosilicate glassy component present in the FA. In the FA/MKPC binders, the Al^{IV} band is slightly deshielded compared to the unreacted FA, with a chemical shift centred at 50 ppm. In alkali-activated fly ash systems, the Al^{IV} region has been observed to sharpen due to the formation of a sodium aluminosilicate hydrate (N-A-S-H) type gel [39] but major differences were not observed in the lineshape of the spectrum in this region (Fig. 7B) suggesting that in the current study, the formation of typical alkali-activated fly ash phases did not occur. Formation of a new, low intensity band in the Al^{VI} region (centred at 14 ppm), and a slight increase in the intensity of the main Al^{VI} , centred at -5 ppm, are observed. These changes may be assigned to the secondary reaction product forming in the FA/MKPC binder; however, the paramagnetic relaxation of the NMR signal associated with the high Fe content of the fly ash limits the resolution achievable. Similarly to the GBFS/MKPC binder (Fig. 7A), the chemical shift changes do not correspond to the formation of aluminium hydroxide polymorphs and aluminosilicates [44], as they have not been identified in these binders, neither through XRD (Fig. 1) nor through thermogravimetry [24]. The ^{27}Al MAS NMR spectra (Fig. 7) have conclusively identified chemical changes to both the octahedral and tetrahedral aluminium environments in SCMs when utilised in MKPC binders. The data presented provides evidence for hypothesis of Wilson et al. [48] regarding the reaction of FA aluminosilicate glass with phosphoric acid to form an aluminium phosphate phase. This suggests that it is likely an aluminium phosphate phase was formed within the MKPC matrix.

Cross-polarisation (CP) NMR can be applied to examine the $^{31}\text{P}\{^1\text{H}\}$ interactions within a sample, in conjunction with information from ^{31}P MAS spectra. For GBFS/MKPC; the CP/MAS NMR (Fig. 8A) shows a sharp resonance at 6.2 ppm in the orthophosphate region, which is associated with struvite-K. The low intensity broad signal centred at 3.6 ppm corresponds to KH_2PO_4 (spectrum not shown), in agreement with previously reported values [49]. KH_2PO_4 was used as a precursor to produce MKPC, and its presence in residual form indicates that the reaction did not proceed to completion, consistent with the identification of residual MgO by XRD. Struvite-K is an isostructural analogue of struvite, and the ^{31}P chemical shift of struvite-K observed in the current study correlates well with that of struvite at 6.1 ppm [50].

The $^{31}\text{P}\{^1\text{H}\}$ CP/MAS NMR spectrum of FA/MKPC (Fig. 8B) was very similar to that of the GBFS/MKPC binder. However, there appeared to

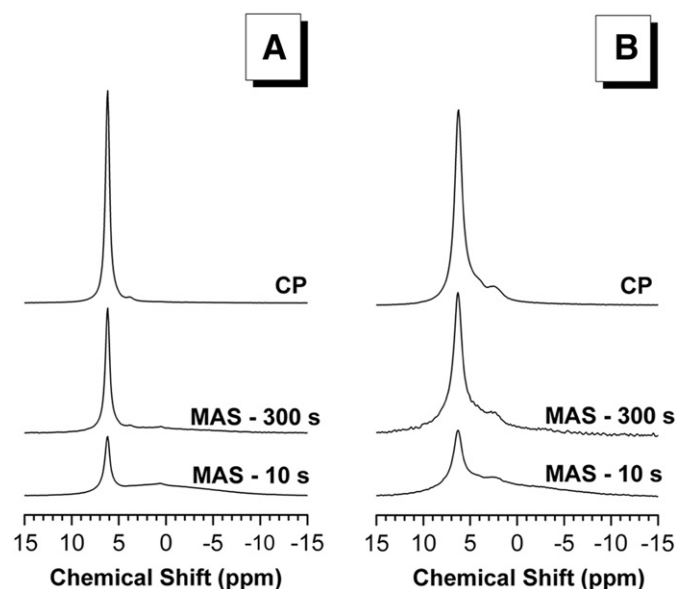


Fig. 8. ^{31}P MAS and CP/MAS NMR spectra (9.4 T, 10 kHz) for: (A) GBFS/MKPC, MAS at relaxation times of 10 and 300 s, and $^{31}\text{P}\{^1\text{H}\}$ CP/MAS at a relaxation time of 1 s; (B) FA/MKPC, MAS at relaxation times of 10 and 300 s, and $^{31}\text{P}\{^1\text{H}\}$ CP/MAS at a relaxation time of 1 s.

be an additional low intensity $^{31}\text{P}\{^1\text{H}\}$ signal located as a shoulder on the crystalline struvite-K peak, centred at 4 ppm, which may be related to an amorphous and/or partially substituted struvite-K phase; the identification of this peak is not yet entirely clear. ^{31}P MAS NMR experiments conducted at different relaxation times (10 and 300 s) enabled identification of low intensity phosphorus environments that have no $^{31}\text{P}\{^1\text{H}\}$ interactions, and thus do not appear in the CP/MAS spectra. In Fig. 8, the appearance of a broad signal between 4 to -4 ppm was observed for both the GBFS/MKPC and FA/MKPC binders. This is indicative of an amorphous phosphorus environment within these systems, and the feature appeared to be slightly more intense in the FA/MKPC binder than the GBFS/MKPC binder. The fact that this does not appear in the ^{31}P CP spectra indicates that it is related to a phosphorus environment that has no intimate interaction with hydrogen, and therefore cannot be attributed to struvite-K.

Based on the chemistry of the binder, it is a logical progression to postulate that the changes observed in the ^{31}P spectra correspond with the additional octahedral Al signal observed in the ^{27}Al spectra (Fig. 7). However, the ^{31}P MAS NMR spectra (Fig. 8) for both FA/MKPC and GBFS/MKPC, do not exhibit resonances necessary to satisfy a Al-P relationship within these systems, which would be in the range of -15 to -35 ppm [25]. Furthermore, multinuclear experiments intended to analyse Al-P interactions in these systems did not show any identifiable signals. It is therefore only possible to state that an amorphous orthophosphate environment exists in both binders but without measurable aluminium interactions.

In the ^{29}Si MAS NMR spectrum of the unreacted GBFS shown in Fig. 9A, a broad resonance centred at -75 ppm was observed, consistent with the glassy fraction and the minor åkermanite present in the slag [37]. The spectrum of the GBFS/MKPC binder (Fig. 9A) has a similar lineshape to that of the unreacted slag; however, the formation of an additional broad band between -90 to -112 ppm was observed. Chemical shifts in this range of values are known to correspond to highly cross-linked Q^4 type sites [52]. This secondary band indicates that during the partial dissolution of GBFS, Al preferentially reacts with P to produce the aluminium phosphate phase discussed above, as identified via ^{27}Al and ^{31}P MAS NMR experiments, leaving the Si to form a highly cross-linked Si-rich type phase, which is highly intermixed with the main binding matrix, as the solubility of Si is low at near-neutral pH.

The broad asymmetric ^{29}Si resonance observed between -76 and -122 ppm, centred at -102 ppm, for the FA sample (Fig. 9B) is consistent with the wide variety of Si environments present in the amorphous and crystalline phases in fly ash: a combination of quartz (~ -107 ppm) [53], mullite (~ -86 ppm) [47], and the vitreous fraction [54]. The FA/MKPC sample also displayed a broad resonance, between -80 and -124 ppm, centred at -103 ppm, however, unlike the GBFS/MKPC binder no significant changes were observed in the ^{29}Si MAS NMR resonances.

High-field MAS NMR experiments for ^{25}Mg and ^{39}K nuclei were conducted on the GBFS/MKPC binder to explore any transformation in the chemical environments of these elements and are shown in Figs. 10 and 11, respectively. Unfortunately, it was not possible to study these nuclei in the FA/MKPC binder due to the relatively high iron content of the fly ash (9.34% by XRF oxide analysis, Table 1). Table 4 defines the quadrupolar parameters; isotropic chemical shift (δ_{iso}), quadrupolar coupling constant (C_Q) and asymmetry (η_Q) used to simulate the spectra for the GBFS/MKPC binder as shown in Figs. 10 and 11.

Fig. 10 identifies two ^{25}Mg MAS NMR environments within the GBFS/MKPC, which are related to struvite-K (M2) and excess MgO (M1) respectively. The isotropic chemical shift, δ_{iso} , of MgO was calculated to be 26.4 ppm, which is consistent with data reported in the literature [55]. MgO is octahedrally coordinated and highly symmetrical, and therefore does not experience strong quadrupolar effects. The GBFS/MKPC binder showed a similar ^{25}Mg MAS NMR spectrum to pure synthetic struvite-K, $\text{MgKPO}_4 \cdot 6\text{H}_2\text{O}$ [56], in which Mg was found to be octahedrally coordinated within the crystal structure, represented

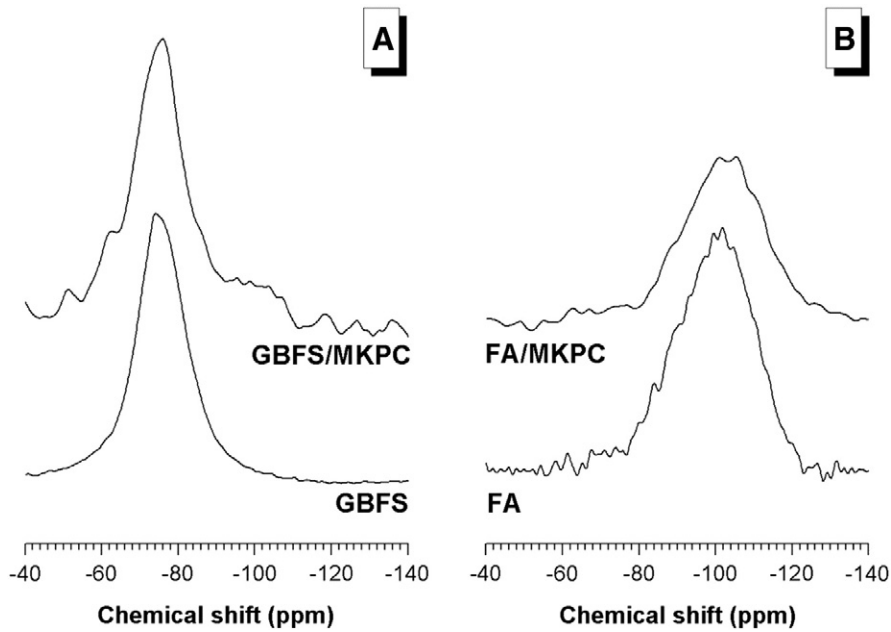


Fig. 9. ^{29}Si MAS NMR spectra (9.4 T, 6.8 kHz) of (A) unreacted GBFS and GBFS/MKPC hardened paste, and (B) unreacted FA and FA/MKPC hardened paste.

by a single resonance with $\delta_{\text{iso}} = -1.0$ ppm, as $\text{Mg}(\text{OH})_2$. The quadrupolar parameters determined for struvite-K are comparable to those reported for struvite in the literature [57].

Åkermanite ($\text{Ca}_2\text{MgSi}_2\text{O}_7$), identified as the only identifiable crystalline phase in GBFS (Fig. 2) should have a single resonance at a chemical shift of 47 ppm [55], however, this region overlaps with the much stronger signal of struvite-K. Due to the low content of åkermanite in the binder it was not possible to distinguish this resonance in Fig. 10. The ^{25}Mg MAS NMR spectrum is described very accurately by the combination of MgO and struvite-K peaks, which suggests that magnesium does not take part in the formation of the secondary reaction products forming within the GBFS/MKPC binder.

The ^{39}K MAS NMR spectrum of the GBFS/MKPC binder (Fig. 11) was found to exhibit a dominant peak assigned to struvite-K. This peak has an isotropic chemical shift of -73 ppm (K1), which is comparable to that reported for struvite-K system [56]. The struvite-K potassium environment undergoes a quadrupolar distortion in the peak shape, which can be used to determine the quadrupolar parameters via an empirical

fitting method. This method utilised experimental data from a pure struvite-K sample [56] and was fitted using TopSpin 3.2 [27] by varying the quadrupolar isotropic shift, asymmetry and line broadening parameters to achieve the best fit.

The simulation in Fig. 11, suggests the presence of a secondary K environment (K2) which exists downfield of the main struvite-K. The K2 phase has been estimated to have an isotropic chemical shift of -107.7 ppm (Fig. 11), and it is possible to confidently conclude that the K2 phase was not associated with free hydrated K^+ ions, which would have a resonance at 0 ppm [26]. Attempts to fit the lineshape with dispersions in quadrupole coupling parameters, consistent solely with a disordered K environment, were unsuccessful. Also, a direct comparison between the ^{39}K MAS NMR spectra of GBFS/MKPC and pure struvite-K (Fig. 12) highlighted the presence of the low intensity shoulder, which cannot be replicated using the struvite-K quadrupolar parameters, even when significantly varied. Therefore, it is suggested that the K2 environment must be incorporated within a secondary (or tertiary) phase in the GBFS/MKPC binder. Certain potassium feldspars (KAlSi_3O_8) exhibit ^{39}K MAS NMR resonances within the region of the

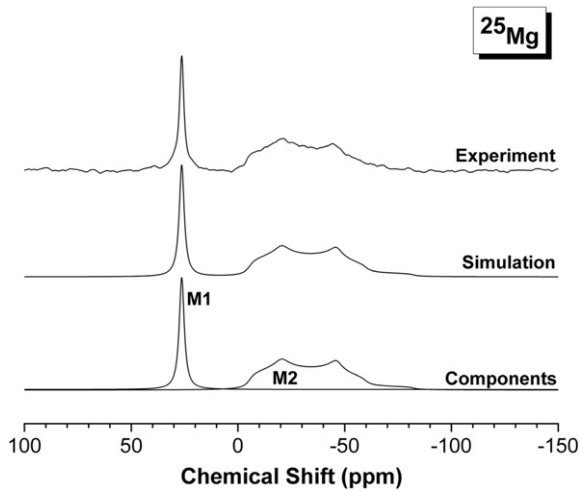


Fig. 10. ^{25}Mg NMR spectrum (19.96 T, 10.0 kHz) of GBFS/MKPC, simulations were performed considering the second-order quadrupolar interaction for the central transition only.

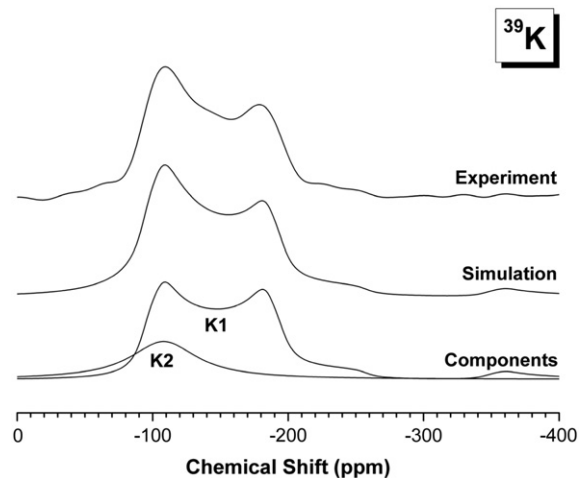


Fig. 11. ^{39}K NMR spectra (19.96 T, 15.0 kHz) of GBFS/MKPC, simulations were performed considering the second-order quadrupolar interaction for the central transition only.

Table 4

NMR quadrupolar parameters for sites calculated in GBFS/MKPC samples using high-field ^{25}Mg and ^{39}K MAS NMR nuclei experiments and struvite-K NMR parameters. The site number denoted for each nucleus (e.g. $^{25}\text{Mg}1$) represents an arbitrarily assigned number for identification purposes, not the atomic position in the crystal structure.

Compound	Nuclei site	Experimental NMR		
		δ_{iso} (ppm) (± 0.1)	C_Q (MHz) (± 0.1)	η_Q (± 0.02)
MgO	$^{25}\text{Mg}1$	26.4	0.0 [55]	N/A
Struvite-K [56]	$^{25}\text{Mg}2$	-1.0	3.8	0.33
GBFS/MKPC	$^{25}\text{Mg}1$	26.4	0.0	N/A
GBFS/MKPC	$^{25}\text{Mg}2$	-1.0	3.8	0.33
Struvite-K [56]	$^{39}\text{K}1$	-73.1	2.2	0.14
GBFS/MKPC	$^{39}\text{K}1$	-73.1	2.2	0.14
GBFS/MKPC	$^{39}\text{K}2$	-107.7	0.1	0.10

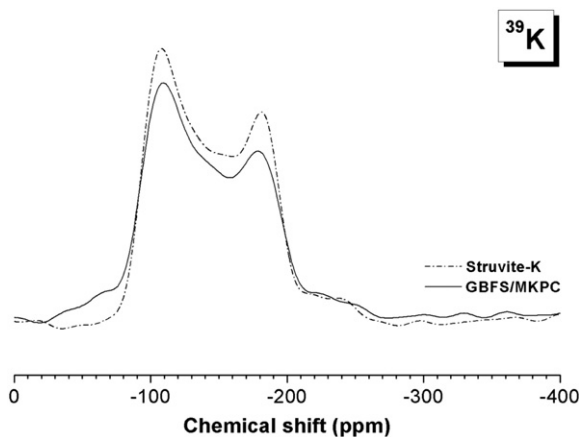


Fig. 12. ^{39}K NMR spectra (19.96 T, 15.0 kHz) of GBFS/MKPC and pure struvite-K.

K2 environment [58–60], whilst their ^{27}Al and ^{29}Si signals at 50 to 65 ppm and -86 to -107 ppm respectively, are consistent with the spectra reported here. Given the aluminosilicate-rich nature of the SCMs and the large quantity of potassium added to these systems as KH_2PO_4 , there could be the potential for poorly crystalline assemblages of this nature. Further work is thus required to fully understand the formation of K–Al–Si secondary phases in these MKPC-SCM binders.

4. Conclusions

The principal role of FA and GBFS in blended MKPC binders is as a filler and diluent. However, microstructural characterisation and multi-nuclear NMR spectra indicated dissolution of the aluminosilicate glassy fractions of both FA and GBFS under the near-neutral pH conditions prevailing within MKPC binders. This has been unambiguously demonstrated for the first time in this contribution. The ^{27}Al and ^{29}Si MAS NMR do not show the formation of C-(A)-S-H gels, as reported in the literature, which is a clear difference between the behaviour of these SCMs under near-neutral pH conditions compared to the reaction products formed through their hydration at high pH. This suggests that the latent hydraulic nature of the slag and pozzolanic nature of the fly ash are not being activated within the near-neutral pH conditions of MKPC binders. Therefore, the chemical changes identified through SEM and NMR investigations are the result of dissolution of the Al and Si from the GBFS and FA particles, induced by the phosphate species present in the MKPC formulations. The secondary products forming in MKPC blended with FA and GBFS are highly enriched in Al and Si, which could potentially lead to the formation of a potassium aluminosilicate phase. The additional phases formed through these interactions may enhance overall densification and potentially increase the durability of MKPC binders. NMR spectra were provided for the first time to

report the true isotropic chemical shift and quadrupolar parameters for the ^{25}Mg and ^{39}K nuclei present in GBFS/MKPC binders. Further work is ongoing, employing multi-nuclear experiments to clarify the existence of both a potassium aluminosilicate phase and an amorphous orthophosphate phase, as proposed from the NMR spectra reported.

Acknowledgements

LJG is grateful to the Nuclear Decommissioning Authority for provision of a PhD bursary and to Dr. Nick C. Collier for industrial supervision (National Nuclear Laboratory). NCH wishes to acknowledge the Royal Academy of Engineering and the Nuclear Decommissioning Authority for funding (R/124464-11-1). NCH and SAW are grateful to EPSRC for provision of a CDT PhD studentship under grant reference: EP/G037140/1. CLC is grateful to the University of Sheffield for the award of a Vice Chancellor's Fellowship. Solid-state NMR spectra (^{27}Al , ^{29}Si , ^{31}P) were obtained at the EPSRC UK National Solid-state NMR Service at Durham, and we thank Dr David Apperley for his generous assistance in collection and interpretation of the results. The UK 850 MHz Solid-State NMR Facility used in this research (^{25}Mg , ^{39}K) was funded by EPSRC and BBSRC, as well as the University of Warwick including via part funding through Birmingham Science City Advanced Materials Projects 1 and 2 supported by Advantage West Midlands (AWM) and the European Regional Development Fund (ERDF). The input of Dr Dinu Iuga in conducting the experiments and the assistance of Dr John V. Hanna in data interpretation at that facility are also gratefully acknowledged.

References

- [1] A.D. Wilson, J.W. Nicholson, *Acid-Base Cements: Their Biomedical and Industrial Applications*, Cambridge University Press, Cambridge, UK, 1993.
- [2] M. Mathew, L.W. Schroeder, Crystal structure of a struvite analogue, $\text{MgKPO}_4 \cdot 6\text{H}_2\text{O}$, *Acta Crystallogr. B* 35 (1979) 11–13.
- [3] S. Graeser, W. Postl, H.-P. Bojar, P. Berlepsch, T. Armbruster, T. Raber, K. Ettinger, F. Walter, Struvite-(K), $\text{KMgPO}_4 \cdot 6\text{H}_2\text{O}$, the potassium equivalent of struvite—a new mineral, *Eur. J. Mineral.* 20 (2008) 629–633.
- [4] A.S. Wagh, *Chemically Bonded Phosphate Ceramics – 21st Century Material with Diverse Applications*, Elsevier, Oxford, UK, 2004.
- [5] F. Qiao, C.K. Chau, Z. Li, Property evaluation of magnesium phosphate cement mortar as patch repair material, *Constr. Build. Mater.* 24 (2010) 695–700.
- [6] A. Covill, N.C. Hyatt, J. Hill, N.C. Collier, Development of magnesium phosphate cements for encapsulation of radioactive waste, *Adv. Appl. Ceram.* 110 (2011) 151–156.
- [7] A.S. Wagh, R. Strain, S.Y. Jeong, D. Reed, T. Krause, D. Singh, Stabilization of rocky flats Pu-contaminated ash within chemically bonded phosphate ceramics, *J. Nucl. Mater.* 265 (1999) 295–307.
- [8] G. Mestres, M.P. Ginebra, Novel magnesium phosphate cements with high early strength and antibacterial properties, *Acta Biomater.* 7 (2011) 1853–1861.
- [9] Q. Yang, X. Wu, Factors influencing properties of phosphate cement-based binder for rapid repair of concrete, *Cem. Concr. Res.* 29 (1999) 389–396.
- [10] Q. Yang, B. Zhu, X. Wu, Characteristics and durability test of magnesium phosphate cement-based material for rapid repair of concrete, *Mater. Struct.* 33 (2000) 229–234.
- [11] Z. Liu, G. Qian, J. Zhou, C. Li, Y. Xu, Z. Qin, Improvement of ground granulated blast furnace slag on stabilization/solidification of simulated mercury-doped wastes in chemically bonded phosphate ceramics, *J. Hazard. Mater.* 157 (2008) 146–153.
- [12] A.S. Wagh, S.Y. Jeong, D. Singh, High strength phosphate cement using industrial byproduct ashes, *Proceedings of 1st International Conference on High Strength Concrete*, United Engineering Foundation Inc., Kona, HI, 1997, pp. 542–553.
- [13] R. Neiman, A.C. Sarma, Setting and thermal reactions of phosphate investments, *J. Dent. Res.* 59 (1980) 1478–1485.
- [14] Y. Li, B. Chen, Factors that affect the properties of magnesium phosphate cement, *Constr. Build. Mater.* 47 (2013) 977–983.
- [15] Z. Ding, Z. Li, Effect of aggregates and water contents on the properties of magnesium phospho-silicate cement, *Cem. Concr. Compos.* 27 (2005) 11–18.
- [16] F. Xing, Z. Ding, Z. Li, Study of potassium-based magnesium phosphate cement, *Adv. Cem. Res.* 23 (2011) 81–87.
- [17] F. Xing, Z. Ding, Z. Li, Effect of additives on properties of magnesium phosphosilicate cement, *Adv. Cem. Res.* 23 (2011) 69–74.
- [18] L. Johansson, J.P. Gustafsson, Phosphate removal using blast furnace slags and opoka-mechanisms, *Water Res.* 34 (2000) 259–265.
- [19] N.M. Ageyi, C.A. Strydom, J.H. Potgieter, The removal of phosphate ions from aqueous solution by fly ash, slag, ordinary Portland cement and related blends, *Cem. Concr. Res.* 32 (2002) 1889–1897.
- [20] S. Lu, S. Bai, H. Shan, Mechanisms of phosphate removal from aqueous solution by blast furnace slag and steel furnace slag, *J. Zhejiang Univ. (Sci.) A* 9 (2008) 125–132.

- [21] British Standards Institute, Fly Ash for Concrete, Part 1: Definition, Specifications and Conformity Criteria, BS EN, 2012. 450–451.
- [22] D.A. Hall, R. Stevens, B. El-Jazairi, The effect of retarders on the microstructure and mechanical properties of magnesia–phosphate cement mortar, *Cem. Concr. Res.* 31 (2001) 455–465.
- [23] E. Soudée, J. Péra, Influence of magnesia surface on the setting time of magnesia–phosphate cement, *Cem. Concr. Res.* 32 (2002) 153–157.
- [24] L.J. Gardner, C.L. Corkhill, S.A. Bernal, N.C. Collier, J.L. Provis, N.C. Hyatt, The effect of water content on blended magnesium potassium phosphate cement binders for radioactive waste encapsulation, 2015. (manuscript in preparation).
- [25] K.J.D. MacKenzie, M.E. Smith, *Multinuclear Solid-State NMR of Inorganic Materials*, Elsevier Science, Oxford, UK, 2002.
- [26] P. Duxson, J.L. Provis, G.C. Lukey, J.S.J. van Deventer, F. Separovic, Z.H. Gan, ^{39}K NMR of free potassium in geopolymers, *Ind. Eng. Chem. Res.* 45 (2006) 9208–9210.
- [27] Bruker, TopSpin 3.2, 2013.
- [28] A. Covill, Cementing change in nuclear waste, *Mater. World Mag.* 18 (2010) 23–25.
- [29] J.L. Provis, P. Duxson, J.S.J. van Deventer, The role of particle technology in developing sustainable construction materials, *Adv. Powder Technol.* 21 (2010) 2–7.
- [30] C.K. Chauhan, P.M. Vyas, M.J. Joshi, Growth and characterization of struvite-K crystals, *Cryst. Res. Technol.* 46 (2011) 187–194.
- [31] S. Zhang, H. Shi, S. Huang, P. Zhang, Dehydration characteristics of struvite-K pertaining to magnesium potassium phosphate cement system in non-isothermal condition, *J. Therm. Anal. Calorim.* 111 (2013) 35–40.
- [32] S. Diamond, Particle morphologies in fly ash, *Cem. Concr. Res.* 16 (1986) 569–579.
- [33] A. Fernández-Jiménez, A. Palomo, Nanostructure/microstructure of fly ash geopolymers, in: J.L. Provis, J.S.J. van Deventer (Eds.), *Geopolymers: Structures, Processing, Properties and Industrial Applications*, Woodhead, Cambridge, UK, 2009, pp. 89–117.
- [34] J.L. Provis, J.S.J. van Deventer, *Geopolymers: Structures, Processing, Properties and Industrial Applications*, Woodhead, Cambridge, UK, 2009.
- [35] R.R. Lloyd, J.L. Provis, J.S.J. van Deventer, Microscopy and microanalysis of inorganic polymer cements. 1: Remnant fly ash particles, *J. Mater. Sci.* 44 (2009) 608–619.
- [36] B.G. Kutchko, A.G. Kim, Fly ash characterization by SEM-EDS, *Fuel* 85 (2006) 2537–2544.
- [37] R.J. Kirkpatrick, MAS NMR spectroscopy of minerals and glasses, in: F.C. Hawthorne (Ed.), *Spectroscopic Methods in Mineralogy and Geology*, The Society, 1988, pp. 341–403.
- [38] R.J. Myers, S.A. Bernal, R. San Nicolas, J.L. Provis, Generalized structural description of calcium–sodium aluminosilicate hydrate gels: the cross-linked substituted tobermorite model, *Langmuir* 17 (2013) 5294–5306.
- [39] S.A. Bernal, J.L. Provis, B. Walkley, R. San Nicolas, J.D. Gehman, D.G. Brice, A.R. Kilcullen, P. Duxson, J.S.J. van Deventer, Gel nanostructure in alkali-activated binders based on slag and fly ash, and effects of accelerated carbonation, *Cem. Concr. Res.* 53 (2013) 127–144.
- [40] J. Schneider, M.A. Cincotto, H. Panepucci, ^{29}Si and ^{27}Al high-resolution NMR characterization of calcium silicate hydrate phases in activated blast-furnace slag pastes, *Cem. Concr. Res.* 31 (2001) 993–1001.
- [41] S. Wang, K.L. Scrivener, ^{29}Si and ^{27}Al NMR study of alkali-activated slag, *Cem. Concr. Res.* 33 (2003) 769–774.
- [42] S. Murgier, H. Zanni, D. Gouvenot, Blast furnace slag cement: a ^{29}Si and ^{27}Al NMR study, *C.R. Chim.* 7 (2004) 389–394.
- [43] J. McManus, S.E. Ashbrook, K.J.D. MacKenzie, S. Wimperis, ^{27}Al multiple-quantum MAS and $^{27}\text{Al}\{^1\text{H}\}$ CPMAS NMR study of amorphous aluminosilicates, *J. Non-Cryst. Solids* 282 (2001) 278–290.
- [44] E. Lippmaa, A. Samoson, M. Mägi, High-resolution ^{27}Al NMR of aluminosilicates, *J. Am. Chem. Soc.* 108 (1986) 1730–1735.
- [45] J. Skibsted, E. Henderson, H.J. Jakobsen, Characterization of calcium aluminate phases in cements by ^{27}Al MAS NMR spectroscopy, *Inorg. Chem.* 32 (1993) 1013–1027.
- [46] H. He, J. Guo, J. Zhu, P. Yuan, C. Hu, ^{29}Si and ^{27}Al MAS NMR spectra of mullites from different kaolinites, *Spectrochim. Acta A* 60 (2004) 1061–1064.
- [47] L.H. Merwin, A. Sebald, H. Rager, H. Schneider, ^{29}Si and ^{27}Al MAS NMR spectroscopy of mullite, *Phys. Chem. Miner.* 18 (1991) 47–52.
- [48] A. Wilson, The chemistry of dental cements, *Chem. Soc. Rev.* 7 (1978) 265–296.
- [49] T. Georgelin, M. Jaber, T. Onfroy, A.-A. Hargrove, F. Costa-Torro, J.-F. Lambert, Inorganic phosphate and nucleotides on silica surface: condensation, dismutation, and phosphorylation, *J. Phys. Chem. C* 117 (2013) 12579–12590.
- [50] S.N. Scrimgeour, J.A. Chudek, G.A. Cowper, C.H. Lloyd, ^{31}P solid-state MAS-NMR spectroscopy of the compounds that form in phosphate-bonded dental casting investment materials during setting, *Dent. Mater.* 23 (2007) 934–943.
- [51] C. Jaeger, F. Hemmann, EASY: a simple tool for simultaneously removing background, deadtime and acoustic ringing in quantitative NMR spectroscopy—part I: basic principle and applications, *Solid State Nucl. Magn. Reson.* 57–58 (2014) 22–28.
- [52] G. Engelhardt, D. Michel, *High-Resolution Solid-State NMR of Silicates and Zeolites*, John Wiley & Sons, Chichester, UK, 1987.
- [53] E. Lippmaa, M. Mägi, A. Samoson, G. Engelhardt, A.R. Grimmer, Structural studies of silicates by solid-state high-resolution ^{29}Si NMR, *J. Am. Chem. Soc.* 102 (1980) 4889–4893.
- [54] A. Palomo, S. Alonso, A. Fernández-Jiménez, I. Sobrados, J. Sanz, Alkaline activation of fly ashes: NMR study of the reaction products, *J. Am. Ceram. Soc.* 87 (2004) 1141–1145.
- [55] P.J. Pallister, I.L. Moudrakovski, J.A. Ripmeester, Mg-25 ultra-high field solid state NMR spectroscopy and first principles calculations of magnesium compounds, *Phys. Chem. Chem. Phys.* 11 (2009) 11487–11500.
- [56] L.J. Gardner, S.A. Bernal, S.A. Walling, C.L. Corkhill, J.L. Provis, N.C. Hyatt, Multinuclear characterisation of synthetic struvite-K, $\text{MgKPO}_4\cdot 6\text{H}_2\text{O}$, a natural analogue of struvite, 2015. (manuscript in preparation).
- [57] D. Laurencin, C. Gervais, H. Stork, S. Krämer, D. Massiot, F. Fayon, ^{25}Mg solid-state NMR of magnesium phosphates: high magnetic field experiments and density functional theory calculations, *J. Phys. Chem. C* 116 (2012) 19984–19995.
- [58] V.F.F. Barbosa, K.J.D. MacKenzie, Synthesis and thermal behaviour of potassium silicate geopolymers, *Mater. Lett.* 57 (2003) 1477–1482.
- [59] J.F. Stebbins, L.-S. Du, S. Kroeker, P. Neuhoff, D. Rice, J. Frye, H.J. Jakobsen, New opportunities for high-resolution solid-state NMR spectroscopy of oxide materials at 21.1- and 18.8-T fields, *Solid State Nucl. Magn. Reson.* 21 (2002) 105–115.
- [60] L. Sánchez-Muñoz, J. Sanz, I. Sobrados, Z. Gan, Medium-range order in disordered K-feldspars by multinuclear NMR, *Am. Mineral.* 98 (2013) 2115–2131.